MULTI-SENSOR INTEGRATION ONBOARD A UAV-BASED MOBILE MAPPING SYSTEM FOR AGRICULTURAL MANAGEMENT

*Magdy Elbahnasawy, Tamer Shamseldin, Radhika Ravi, Tian Zhou, Yun-Jou Lin, Ali Masjedi, Evan Flatt, Melba Crawford, and Ayman Habib**

Lyles School of Civil Engineering, Purdue University, USA

ABSTRACT

Due to the advances in technological and industrial fields, remote sensing has been adopted to a considerable extent in precision agricultural applications. Over the past few years, remote sensing utilized Mobile Mapping Systems (MMS) as the platforms for agricultural data collection. For accurate generation of georeferenced products using such MMSs, there should be a robust calibration approach that can accurately estimate the mounting parameters of the involved sensors, i.e., LiDAR unit, camera, and hyperspectral push-broom scanner. In this paper, we propose novel calibration approaches for various sensors onboard a UAV platform – 1) simultaneous estimation of lever arm and boresight angles relating LiDAR unit and camera to the GNSS/INS unit, and 2) estimation of boresight angles relating hyperspectral push-broom scanner and the GNSS/INS unit.

Index Terms— Calibration, geospatial data, biomass, canopy structure

1. INTRODUCTION

Precision agriculture generally involves better management of farm inputs such as fertilizers, herbicides, seed, fuel (used during tillage, planting, spraying, etc.) by doing the right management practice at the right place and the right time. For agricultural management applications, the increased requirements for geospatial data at a higher spatial resolution and temporal frequency have led to the emergence of low-cost UAVs over manned aircrafts and satellite remote sensing systems for agricultural management. UAVs offer several design and performance advantages over other conventional platforms, such as small size, low weight, low flying height, slow flight speed, low cost, and ease of storage and deployment. For agricultural management, multi-sensor integration onboard UAV-based mobile mapping system provides an efficient approach for manipulation among different sensors information. For example, the integration of passive sensors, including RGB cameras, push-broom hyperspectral (Visible Near Infrared - VNIR and Short Wave Infrared – SWIR), along with (Thermal Infrared - TIR) data can be used in biomass estimation as well as offering additional information on crop water stress status [1], [2]. Furthermore, active sensors, such as LiDAR systems, can directly provide precise and reliable 3D information for the scanned area to be used in producing detailed geometric models and biomass estimations [3]. Due to recent improvements in the accuracy of integrated Global Navigation Satellite Systems (GNSS) and Inertial Navigation Systems (INS), the data captured by both passive and active sensors mounted on UAV can be georeferenced with high spatial accuracy.

Over the past few years, extensive research has been conducted for the calibration of LiDAR-based airborne mobile mapping systems [4], [5]. Similarly, several techniques have been developed to accurately calibrate different types of cameras in order to obtain accurate estimates of their intrinsic and extrinsic parameters [6], [7]. Although many procedures have been developed for LiDAR system calibration and camera calibration separately, the simultaneous calibration of a mapping system consisting of both LiDAR units and cameras is an area of research that is still under exploration. [8] devised a method for automatic extrinsic calibration and sensor fusion for a system comprised of a LiDAR and an optical camera by exploiting the natural alignment of depth and intensity edges. [9] developed an approach for real-time miscalibration detection and correction by using a probabilistic background monitoring algorithm. In the current study, we propose a calibration approach for an integrated LiDAR and camera system based on the use of conjugate points and linear/planar features in overlapping images and point clouds derived from different flight lines.

For push-broom scanners, significant research has been dedicated towards establishing reliable boresight calibration strategies. [10] proposed a boresight calibration approach for airborne and space borne push-broom scanners. Here, using the interior orientation parameters, GNSS/INS georeferencing parameters, nominal lever arm components and boresight angles, and an available Digital Elevation Model (DEM), the image points corresponding to established GCPs were projected onto the DEM and boresight angles were estimated by minimizing the differences between the GCPs and the projected ground coordinates. The key limitation of the above approaches is the need for having a DEM of the covered area as well as some GCPs. In this paper, the hyperspectral push-broom scanner system is calibrated by a rigorous approach using tie features by enforcing an optimal intersection of the light rays connecting the perspective centers of the imaging scanner, object point, and the respective image points.

Acknowledgment: This work was supported in part by the Advanced Research Projects Agency-Energy, U.S. Department of Energy, under Award Number DE-AR0000593.

An experimental setup is used to evaluate the performance of the proposed calibration procedure for UAV-based integrated LiDAR and camera system through the a-posteriori variance factor of the Least Squares Adjustment (LSA) procedure and the quality of fit of the adjusted LiDAR point cloud and image points to linear/planar surfaces before and after the calibration process. The accuracy of the boresight calibration strategy for hyperspectral push-broom scanners is evaluated by using the estimated boresight angles for ortho-rectification of six hyperspectral UAV datasets acquired over an agricultural field. Qualitative and quantitative evaluations of the results have shown significant improvement in the derived orthophotos to a level equivalent to the Ground Sampling Distance (GSD) of the used scanner.

2. SYSTEM INTEGRATION

The LiDAR, RGB, and hyperspectral imagery datasets used in this study are captured by a UAV-based system consisting of DJI M600 as the platform. Currently, due to weight constraints, the sensors were mounted on 2 different platforms – one carrying a Velodyne VLP-16 laser scanner and a Sony Alpha 7R (ILCE-7R) camera, and the other carrying a Headwall Nano-Hyperspec push-broom scanner. Both the systems consist of an APX-15 V2 as the GNSS/INS unit, considering its weight and accuracy. A Raspberry Pi module is used to store the LiDAR data whereas the RGB camera and hyperspectral push-broom scanner has its own storage. In case of the platform carrying the hyperspectral push-broom scanner, a DJI Ronin MX 3-axis brushless gimbal stabilizer was used on the airframe. The Velodyne VLP-16 has a typical range accuracy of 3 cm. The Sony Alpha 7R is a 36.4 MP off-the-shelf camera. This selection supports the goal of having maximum image resolution to facilitate accurate orthophoto generation and 3D point cloud reconstruction. The Headwall Nano-Hyperspec has a focal length of 12.7 mm, which corresponds to roughly 3.5 cm GSD when flying at 60 m above ground. It covers 272 spectral bands ranging between 400 nm and 1000 nm with a band width of 2.2 nm. Each scan line contains 640 pixels with a pixel pitch of 7.4 µm. For the APX-15 unit, the post-processing accuracy in position is 2 to 5 cm and the predicted accuracy for the roll/pitch and heading is 0.025 and 0.08˚, respectively. The LiDAR Error Propagation calculator developed by [11] suggests that for a flying height of 20 m (used in this experiment), we should expect an accuracy of around 5-6 cm for the derived point cloud coordinates. The block diagram of the M600 UAV-based MMS, indicating triggering signals, feedback signals, and communication wires/ports between sensors and power connections is shown in Figure 1.

3. MATHEMATICAL MODELS FOR THE SENSORS

In this paper, we propose novel strategies for the calibration of the two different systems – one consisting of a LiDAR unit and a camera, and the other consisting of a hyperspectral push-broom scanner. But before proceeding towards a detailed discussion about the calibration strategies, we first present the mathematical models used for each sensor (frame camera, LiDAR unit, and hyperspectral push-broom scanner) and state the objectives of system calibration, i.e., the unknown parameters that need to be accurately estimated for each of the systems.

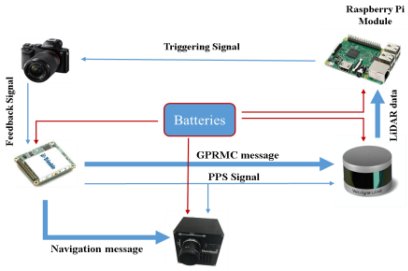

Fig. 1 Integration scheme for the M600 UAV-based system

Frame Camera: A typical GNSS/INS-assisted frame camera system would involve 3 coordinate systems (i.e., mapping frame, IMU body frame, and camera coordinate frame). A given point, $\boldsymbol{I}$, captured in an image as point, $\boldsymbol{i}$, from a camera onboard a mobile mapping system can be reconstructed in the mapping coordinate system using Equation 1. Here, $r_i^C(t)$ denotes the distortion-free coordinates of a point, $\boldsymbol{i}$, in an image captured by camera, C, relative to the camera coordinate system. The camera (C) is related to the IMU body frame by a rigidly defined lever arm, r_C^b, and boresight matrix, R_C^b. Finally, each point, $\boldsymbol{i}$, in an image captured by camera, C, at time, t, has a scaling factor associated with it, which is denoted by $\lambda(i, C, t)$. The GNSS/INS integration provides the time dependent position, $r_b^m(t)$, and rotation, $R_b^m(t)$, relating the mapping frame and IMU body frame coordinate systems, according to the optimized solution from the available GNSS and inertial measurements. The unknowns that need to be calibrated in case of a frame camera include the lever arm, r_C^b, the boresight angles constituting R_C^b, and the scaling factors, $\lambda(i, C, t)$ for all the image points used for calibration.

$$r_I^m = r_b^m(t) + R_b^m(t)\, r_c^b + \lambda(i, C, t)\, R_b^m(t)\, R_C^b\, r_i^C(t) \quad (1)$$

LiDAR Unit: A typical LiDAR system would involve 3 coordinate systems (i.e., mapping frame, IMU body frame, and laser unit frame). A given point, $\boldsymbol{I}$, acquired from a mobile mapping system equipped with a laser scanner can be reconstructed in the mapping coordinate system using Equation 2. Here, $r_I^{lu}(t)$ denotes the coordinates of a 3D point relative to the laser unit coordinate system. The laser unit (lu) is related to the IMU body frame by a rigidly defined lever arm, r_{lu}^b, and boresight matrix, R_{lu}^b. Here, the unknowns to be estimated during calibration are the lever arm, r_{lu}^b, and the boresight angles constituting the matrix, R_{lu}^b.

$$r_I^m = r_b^m(t) + R_b^m(t)\, r_{lu}^b + R_b^m(t)\, R_{lu}^b\, r_I^{lu}(t) \quad (2)$$

Hyperspectral Push-broom Scanner: The calibration approach used for a hyperspectral push-broom scanner is based on a collinearity equation model, where the image coordinates are represented as a function of the GNSS/INS position and orientation, ground coordinates of the tie features, lever arm components, and the boresight angles, as represented by Equation 3. Here, the lever arm is assumed to be measured accurately, while the boresight angles need to be estimated. To eliminate the unknown scale factor λ_i from Equation 3, the first and second rows can be divided by the third one, thus resulting in two equations involving the unknown boresight angles $(\Delta\omega, \Delta\varphi, \Delta\kappa)$ and the ground coordinates of the tie features, r_I^m.

$$r_i^c = {}^1/_{\lambda_i} R_b^c \{ R_m^b(t) [r_I^m - r_b^m(t)] - r_c^b \} \quad (3)$$

4. SYSTEM CALIBRATION STRATEGIES

An integrated LiDAR and camera system calibration aims to simultaneously estimate all the system parameters so as to minimize the discrepancies among conjugate points, linear features, and/or planar features obtained from different laser scanners, cameras, and/or flight lines. In this research, we developed a point-pairing-based technique for bundle adjustment of images as well as the integration of LiDAR and image points in order to conduct a simultaneous calibration of the two sensors. This is achieved by imposing an equality constraint on the 3D mapping frame coordinates computed for different LiDAR/image points representing the same object point by pairing them together. However, owing to the irregular distribution of LiDAR points leading to inaccurate point-to-point correspondence, this research proposes an incorporation of linear/planar features which are represented in LiDAR scans/images as a sequence of pseudo-conjugate points lying along the features. The equality constraint is then updated using a modified weight matrix for each feature to ensure the elimination of non-random discrepancy along the feature to which a point pair belongs. A detailed analysis on the contribution of pairings for different types of features (points, lines, and planes) indicates that the following pairing scheme is designated to be optimal in order to conduct an integrated LiDAR and camera system calibration:

- Image-to-image conjugate point pairing,
- LiDAR-to-LiDAR and LiDAR-to-image pairings of pseudo-conjugate points belonging to corresponding linear features,
- LiDAR-to-LiDAR pairings of pseudo-conjugate points along corresponding planar features, and
- LiDAR-to-image pairings of pseudo-conjugate points belonging to corresponding planar features along with image-to-image conjugate point pairs for the same feature.

This research carries out an iterative calibration procedure where the discrepancy among extracted points/features is minimized using a modified weight matrix to derive mounting parameters through a Least Squares Adjustment (LSA) process.

The proposed calibration approach for a hyperspectral push-broom scanner is based on using identified tie features in the push-broom scanner scenes to estimate the boresight angles. The boresight angles are estimated by enforcing the coplanarity constraint relating conjugate features in overlapping push-broom hyperspectral scenes. In this case, since one is dealing with a non-linear model in the involved unknowns, as given in Equation 3, an iterative LSA procedure is used starting from approximate values of the unknowns. For a tie point that is observed in n scenes will lead to 2n equations in 6 unknowns. This work also derives an optimal/minimal configurations of the flight line and tie point distribution to allow for reliable estimate of the boresight angles and ground coordinates of tie points.

5. EXPERIMENTAL RESULTS

Simultaneous LiDAR and Camera Calibration: The dataset collected by the UAV-based system covers sixteen highly reflective boards that can be easily identified as high intensity regions in the airborne LiDAR data, and each of their corners can be distinctly identified and paired in different images. Five hut-shaped target boards are also deployed, with their ridges oriented perpendicular to each other. The two surfaces corresponding to each of these huts are used as planar features for calibration, and their ridges are used as conjugate linear features between the images and the overlapping LiDAR point clouds from different flight lines. In this experiment, the flight path of the UAV comprises ten flight lines at a fixed height of 20 m above the ground, with different directions and lateral distance between them. These flight lines cover the calibration primitives at an approximate speed of 1.5 miles/hr. The camera is set to capture images at an interval of 1.5 sec.

The qualitative evaluation of the calibration results is done in two different ways – (a) Figure 2 showing the alignment in object space by computing the 3D mapping frame coordinates for all the LiDAR and image points; and (b) Figure 3 showing the alignment in image space by evaluating the pixel coordinates for all the LiDAR and image points based on their 3D mapping frame coordinates after calibration. Figures 2 and 3 indicate that the corners of the checkerboard target measured in different images align well with the high intensity LiDAR points. Similarly, the image points along the hut ridge are aligned in 3D with the corresponding LiDAR points.

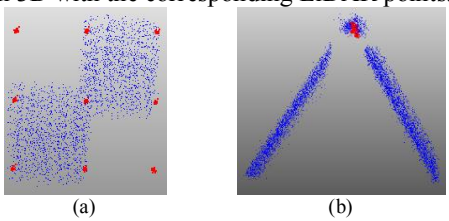

(a) (b)

Fig. 2 Qualitative evaluation of 3D alignment between LiDAR (blue) and image points (red) after calibration: (a) specially designed checkerboard target and its corners, (b) front view of hut-shaped target

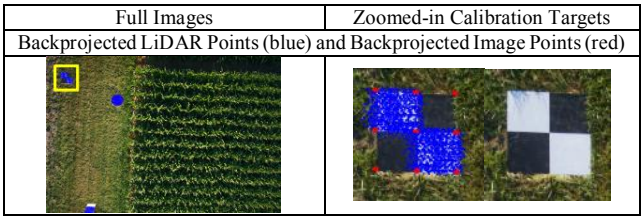

Fig. 3 Qualitative evaluation of 2D alignment between LiDAR data and images after calibration for the UAV-based system

The initial approximations of all the mounting parameters and the final results (along with their standard deviations) after calibration are listed in Table 1. One should note that apart from the vertical lever arm component (ΔZ) of the laser scanner, the planimetric lever arm components ($\Delta X, \Delta Y$) are also fixed (from manual measurements) since different flying heights are required in order to eliminate the correlation between the planimetric lever-arm components and the boresight parameters. The square root of the a-posteriori variance factor ($\hat{\sigma}_o$) representing the average compatibility between all the conjugate and pseudo-conjugate point pairings is 2.07 cm after calibration in this case. This is better than the expected accuracy of around 5-6 cm for a flying height of 20 m according to the accuracies of the hardware involved. The RMSE of normal distance of LiDAR and image points from best-fitting plane/line for extracted features after calibration were found to

lie in the range of 1.5 to 2.5 cm.

Calibration of Hyperspectral Push-broom Scanner: For this study, six datasets were acquired during the summer of 2017. The experimental location is an agricultural test field within the Agronomy Center for Research and Education (ACRE) at Purdue University. Five checkerboard targets, which are used as either tie features or GCPs, were deployed in the field. The ground coordinates of all the checkerboard targets were surveyed by a Topcon GR-5 GNSS receiver. The checkerboard targets are identified in the original hyperspectral scenes and the image point coordinates are measured.

The estimated boresight angles for 15th July were: $\omega = 90.259°, \phi = 0.527°, \kappa = -90.215°$. The accuracy of the estimated boresight angles is qualitatively checked by visually inspecting the ortho-rectified mosaics using the nominal and estimated boresight angles from the different calibration strategies. Figure 4 shows the ortho-rectified mosaics for the July 15th dataset. Visible misalignments in parts A and B while using the nominal boresight angles are quite obvious. Zoomed-in areas at those locations are also included in Figure 4 for closer inspection. These misalignments have been eliminated in the post-calibrated ortho-rectified mosaics.

Derived ground coordinates from the boresight calibration are compared with the surveyed coordinates of the checkerboard targets as well as the coordinates derived using nominal values. The RMSE of the differences along the XYZ directions were reduced from (0.273 m, 0.538 m, 0.870 m) to (0.054 m, 0.035 m, 0.352 m), respectively. This indicates that the calibration strategy had a major impact in improving the planimetric accuracy of derived ground coordinates. The RMSE in the vertical direction is significantly worse than the planimetric RMSE. The relatively worse vertical accuracy as represented by the RMSE is hypothesized to be caused by the intersection geometry for conjugate light rays.

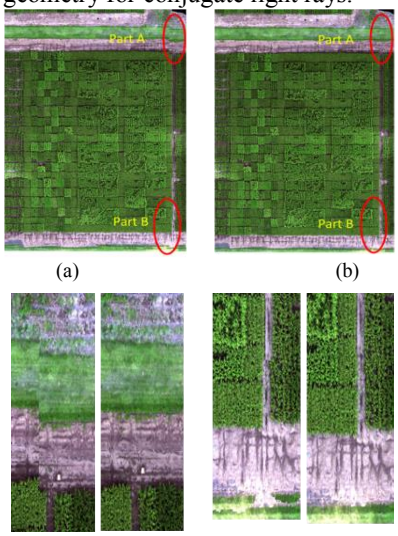

Fig. 4 Generated ortho-rectified mosaics for the July 15th dataset: (a) using nominal boresight angles, (b) using the tie-feature-based rigorous calibration estimates of the boresight angles, (c) and (d) zoomed-in areas for parts A and B, respectively before (left) and after (right) the calibration process.

6. RECOMMENDATIONS FOR FUTURE WORK

In the future, we would target a simultaneous calibration of all the sensors together by pairing point/features from the different sensors. In order to extend this research, we plan to qualitatively and quantitatively analyze the alignment of georeferenced products obtained from each of the sensors onboard the UAV platform, i.e., LiDAR unit, camera, and hyperspectral push-broom scanner. We are going to further analyze the multi-sensor system performance for various applications, such as plant height, canopy cover, and biomass estimation.

TABLE I
MOUNTING PARAMETERS BEFORE AND AFTER CALIBRATION OF THE UAV-BASED SYSTEM

VLP-16 LiDAR Unit Mounting Parameters $(r^b_{Lu'})$ $(R^b_{Lu'})$						
	ΔX (m)	**ΔY (m)**	**ΔZ (m)**	**Δω (°)**	**Δφ (°)**	**Δκ (°)**
Initial	0.020	0	0	0	0	0
Final	0.020	0	0	0.1898	0.3008	-0.0950
Std. Dev.	Fixed	Fixed	Fixed	0.0165	0.0209	0.0340
Sony α7R Camera Mounting Parameters (r^b_C) (R^b_C)						
	ΔX (m)	**ΔY (m)**	**ΔZ (m)**	**Δω (°)**	**Δφ (°)**	**Δκ (°)**
Initial	0.134	-0.037	0.05	180	0	-90
Final	0.134	-0.037	0.0271	179.7720	-0.2339	-90.413
Std. Dev.	Fixed	Fixed	0.0522	0.0389	0.0389	0.0733

7. REFERENCES

[1] Holman, F. H., Riche, A. B., Michalski, A., Castle, M., Wooster, M. J., & Hawkesford, M. J. (2016). High throughput field phenotyping of wheat plant height and growth rate in field plot trials using UAV based remote sensing. *Remote Sensing*, *8*(12), 1031.

[2] Ballesteros, R., Ortega, J. F., Hernandez, D., & Moreno, M. A. (2018). Onion biomass monitoring using UAV-based RGB imaging. *Precision Agriculture*, 1-18.

[3] Hämmerle, M. and Höfle, B., 2014. Effects of reduced terrestrial LiDAR point density on high-resolution grain crop surface models in precision agriculture. *Sensors*, *14*(12), pp.24212-24230.

[4] Habib, A., Kersting, A. P., Shaker, A., & Yan, W. Y. (2011). Geometric calibration and radiometric correction of LiDAR data and their impact on the quality of derived products. *Sensors*, *11*(9), 9069-9097.

[5] Glennie, C., Brooks, B., Ericksen, T., Hauser, D., Hudnut, K., Foster, J., & Avery, J. (2013). Compact multipurpose mobile laser scanning system—Initial tests and results. *Remote Sensing*, *5*(2), 521-538.

[6] Habib, A., Morgan, M., & Lee, Y. R. (2002). Bundle adjustment with self–calibration using straight lines. *The Photogrammetric Record*, *17*(100), 635-650.He, Mengwen, et al. "Pairwise LIDAR calibration using multi-type 3D geometric features in natural scene." *Intelligent Robots and Systems (IROS), 2013 IEEE/RSJ International Conference on*. IEEE, 2013.

[7] Furukawa, Y., & Ponce, J. (2009). Accurate camera calibration from multi-view stereo and bundle adjustment. *International Journal of Computer Vision*, *84*(3), 257-268.

[8] Castorena, J., Kamilov, U. S., & Boufounos, P. T. (2016, March). Autocalibration of LIDAR and optical cameras via edge alignment. In *Acoustics, Speech and Signal Processing (ICASSP), 2016 IEEE International Conference on* (pp. 2862-2866). IEEE.

[9] Levinson, J., & Thrun, S. (2013, June). Automatic Online Calibration of Cameras and Lasers. In *Robotics: Science and Systems* (pp. 24-28).

[10] R. Muller, M. Lehner, R. Muller, P. Reinartz, M. Schroeder, and B. Vollmer, "A program for direct georeferencing of airborne and spaceborne line scanner images," *International Archives of Photogrammetry Remote Sensing and Spatial Information Sciences*, vol. 34, no. 1, pp. 148–153, 2002.

[11] Habib, A., Lay, J., & Wong, C. (2006). Specifications for the Quality Assurance and Quality Control of LIDAR Systems. *Submitted to the Base Mapping and Geomatic Services of British Columbia*. https://engineering.purdue.edu/CE/Academics/Groups/Geomatics/DPRG/files/LIDARErrorPropagation.zip